Electron Microscopy: Its Role in Materials Science

The Mike Meshii Symposuim

Proceedings of a Symposia sponsored by
the Mechanical Behavior of Materials Committee (Jt. ASM-MSCTS) of
the Structural Materials Division (SMD) of
TMS (The Minerals, Metals & Materials Society) with
the Japan Institute of Metals

2003 TMS Annual Meeting
San Diego, California
March 2-6, 2003

Edited by

J.R. Weertman
M. Fine
K. Faber
W. King
P. Liaw

A Publication of
TMS

Electron Microscopy: Its Role in Materials Science (The Mike Meshii Symposium)
Edited by J.R. Weertman, M. Fine, K. Faber, W. King and P. Liaw TMS (The Minerals, Metals & Materials Society), 2003

ELECTRON BACKSCATTER DIFFRACTION FOR STUDIES OF LOCALIZED DEFORMATION*

R.H. Geiss, A. Roshko[1], K.A. Bertness[1], and R.R. Keller

NIST, Materials Reliability Division, 325 Broadway, Boulder, CO 80305
[1]NIST, Optoelectronics Division, 325 Broadway, Boulder, CO 80305

Abstract

Electron backscatter diffraction (EBSD) was used to study localized deformation in two types of constrained-volume materials. We present a study of deformation in narrow aluminum interconnects after low frequency, AC cycling at high current density. Joule heating and differential thermal expansion caused cyclic thermal straining, resulting in thermomechanical fatigue. By quasi *in-situ* testing, we determined the evolution of the crystallography of all grains and boundaries in the interconnect lines. The results allowed us to formulate a mechanistic understanding of the deformation process, including slip line formation and grain growth. In a second study, we analyzed diffraction patterns from selectively oxidized, multilayered AlGaAs/GaAs structures. Elastic strains associated with the oxidation front in multilayered AlGaAs were characterized by EBSD. Pattern sharpness maps revealed the resulting strain field about the oxide growth front, which we compared with finite element simulations. Quantitative strain measurements were made comparing measurements of band widths on processed images.

Introduction

A goal of this paper is to demonstrate two applications of automated EBSD to deformation problems, with demonstrations of results that cannot be easily obtained by other methods. We begin by briefly reviewing how electron backscatter diffraction has been used for deformation studies. EBSD can be used to characterize plastic and elastic deformation in crystalline materials. In each case, the effect of strain on the diffraction pattern is apparent through changes in lattice parameters. For plastic deformation, due to strains associated with crystal defects, the changes are highly localized. For elastic deformation, the changes are generally not as localized. The effects of both types of strain can be seen by changes in the widths and/or sharpnesses of diffraction bands, although elastic distortions can have an additional effect, such as causing zone axes to shift from their undistorted positions.

Plastic deformation has been characterized in numerous investigations by EBSD. Examples include studies of deformation induced by creep [1], nanoindentation [2], and implantation [3]. The approach involves quantifying the extent of pattern sharpness and empirically correlating this to some degree of plasticity. The general idea is that the elastic distortion field about a dislocation will cause the Bragg angle to vary locally, and hence change Kikuchi band widths. Increasing the density of a random distribution of dislocations would then cause a corresponding increase in the distribution of Kikuchi band widths. Similarly, introducing a high density of point defects can cause localized changes in strain, which also affects band widths. Accompanying the changes in band width is a general decrease in pattern contrast with increasing deformation. Eventually, orientation information is lost as lattice disorder becomes extreme. A sensitivity of about ±1 % plastic strain can be achieved using quantification of pattern sharpness.

Plastic deformation and fracture can also be characterized using EBSD through measurements of the orientation dependence of features such as cleavage facets or subgrain formation in the vicinity of cracks. Such studies approach the characterization of deformation at the individual grain or subgrain level, rather than concentrating solely on the distribution of lattice parameters at a given electron beam location. We show in this paper an example of combining the power of automated orientation mapping with the spatial resolution of a field emission scanning electron microscope, SEM, to study submicrometer-level plastic deformation-induced changes in the structure of interconnects. By performing a series of experiments where we alternated EBSD mapping with electrical stressing, we conducted a quasi *in-situ* deformation test with the SEM. The material under study was a patterned aluminum alloy film subjected to thermomechanical fatigue.

Turning our attention to elastic deformation, the most direct means for extracting lattice parameter information from EBSD patterns involves measuring Kikuchi band widths, which are directly proportional to the Bragg angle. However, EBSD has not been widely used in this manner for several reasons. First, relatively low signal-to-noise ratios in patterns detected by film or by cameras optimized for rapid data collection can make distinct Kikuchi band edges impossible to see, except for very low index reflections, which often show poor sensitivity to small strains. Second, there is a significant orientation-independent component to the background of experimental patterns, thereby decreasing the contrast between diffraction band edges and pattern background. Third, most EBSD cameras detect scattering into large solid angles, precluding high resolution observation of small angular changes, such as variations in band width. These factors have combined to limit the practical applicability of this method for the measurement of elastic strain. Recent advances, however, in the use of zone axis (ZA) shifts and image cross-correlation [4] have brought about a renewed interest in the use of electron backscatter diffraction for the determination of elastic strain.

Comparison of ZA positions for an undistorted crystal and a distorted crystal reveals a set of ZA shifts that can be correlated to the degree of distortion in the crystal [4]. This can then be used to extract a strain tensor. Examples of successful application of this method can be found in references [5, 6] for the case of epitaxial $Si_{1-x}Ge_x$ on Si. The sensitivity of this approach, when coupled with cross-correlation methods, is approximately ±0.02 % strain. Michael and Eades [7] have demonstrated that higher order Laue zone (HOLZ) reflections in EBSD patterns can be detected and used to determine the spacing of the reciprocal lattice interlayer in the direction of a zone axis. This is possible provided that the detection system reveals both the fine angular detail and the low contrast inherent to such reflections. In this sense, EBSD patterns can be used in a manner similar to that demonstrated for electron channeling patterns [8], leading to a strain sensitivity approaching ±0.1 %.

In this paper, we report two additional methods for elastic strain characterization. One allows us to measure very large elastic strains (>6 %), which are sometimes present in multilayered semiconductor structures containing selectively oxidized regions; this becomes possible through the use of low-index zero-order diffraction reflections. The other is a mapping of the extent of an elastic distortion field associated with oxidation. This is achievable upon realization of the effects of elastic strain gradients on pattern sharpness.

Experimental

AC Stressing of Al-Si Interconnects

Low frequency AC testing at high current density, was performed on chip-level interconnects to simulate thermal cycling that such structures may undergo during their operational lifetimes.

Such cycling can occur due to powering on and off, energy saving schemes in portable systems, and even during the execution of processor-intensive computer applications.

Samples consisted of single-level, patterned and etched, unpassivated Al-1at.% Si lines of length 800 μm, thickness 0.55 μm, and width 3.3 μm. They were conventionally processed, yielding metal structures with random in-plane orientations about a strong {111} fiber texture. The lines connected two bond pads and were deposited directly onto oxidized silicon. Electrical stressing was carried out in laboratory air at a nominal temperature of 20 °C, with the die held by vacuum onto a large metal platen. Tungsten needle probes were used to make contact to the bond pads. A signal generator was used to supply the lines with sinusoidal currents at 100 Hz, with DC offsets of less than several millivolts. The rms current density used in this work was approximately 12.2 MA/cm^2. The average sample temperature, as monitored using a thermocouple attached directly to the die, indicated a rise of < 10 K during electrical testing. However, the low frequency AC signals led to temperature cycling superimposed onto the average die temperature, with an amplitude of approximately 100 K, at a frequency of 200 Hz, which corresponds to the power cycling input into the line. Thermal expansion mismatch between the metal and substrate then led to cyclic straining, causing damage in the metal by thermomechanical fatigue, as described in [9]. Under the present test conditions, the lifetimes to open circuit failure were approximately 2-4 hours.

We have recently observed that significant changes can occur in the microstructure of the interconnects during very early stages of AC cycling. So we performed quasi *in-situ* AC tests wherein we fully characterized the microstructure of the lines between different stages of electrical testing, using automated EBSD scans. The scans were set up with a Schottky field emission SEM operating at 15 kV. This voltage provided a good compromise between generating sufficient signal from the relatively weakly-scattering aluminum alloy and sampling a small enough information volume to allow detection of crystallographic information from most of the smaller grains in the structure. After briefly exposing the sample to oxygen plasma to minimize carbon-based contaminants in the chamber, we used a step size of 200 nm and limited individual scan times to less than 30 minutes to minimize effects of drift. The entire 800 μm line length and 3.3 μm line width was characterized in this manner. Here, we report the evolution of changes seen after 10, 20, and 40 seconds of testing of the same interconnect, making comparisons to the starting structure.

Phase Transformation-Induced Deformation of AlGaAs/GaAs Multilayers

We are characterizing selectively oxidized AlGaAs/GaAs multilayers as part of a project involving strain control in photonic semiconductors that are used in applications such as vertical cavity surface-emitting lasers. Oxidized Al-containing layers can serve as optical apertures in such devices. Reliability problems can ensue during fabrication of such devices, since the transformation from AlGaAs to aluminum oxide is accompanied by a very large volume contraction. The theoretical contraction exceeds 20%, while TEM-based measurements of the linear contraction seen in cross sections suggest a value of approximately 6.7% [10]. Adjacent layers of GaAs thus also undergo straining, and two potential failure mechanisms become evident: interlayer delamination and strain relaxation by misfit dislocation formation. Both can compromise the functionality of an optical device.

Samples consisted of alternating layers of $Al_xGa_{1-x}As$ (x = 0.90 to 1.00) and GaAs, 80 and 200 nm thick, respectively, grown by molecular beam epitaxy onto GaAs (001) substrates. The Al-containing layers were then oxidized wet-thermally for 5 minutes at 485 °C to form alternating layers of amorphous oxides. For automated EBSD characterization, fresh cross-sectional surfaces were prepared by cleaving surfaces running parallel to the oxide growth direction. The

field emission SEM was operated at an accelerating voltage of 15 kV.. Following oxygen plasma exposure in the SEM, scans were run at a step size of 50 nm.

Results and Discussion

AC Stressing of Al-Si Interconnects

Automated EBSD revealed microstructural changes due to AC stressing that would have been difficult if not impossible to ascertain with other experimental methods. An example is shown in Figure 1, which illustrates a few notable features. The SEM image of a 3.5 μm wide line, in the top figure, shows surface topography that is localized to a particular region of the line, suggesting selectivity in damage formation that may be controlled by localized variations in microstructure. The orientation map, in the bottom figure at the same magnification, confirms that the damage is indeed confined to a single grain. The orientation for that grain is shown schematically to the left and suggests a possible dislocation mechanism that could form slip lines, which likely accounts for the topography. We note that for the geometry of this line, a significant tensile stress in the longitudinal direction is expected.

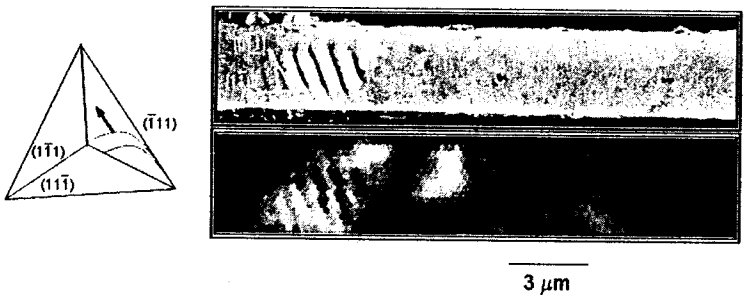

Figure 1: Dislocation mechanism for topography formation induced by AC stressing in Al-1Si.

The sequence of SEM images in Figure 2 shows the development of surface topography that became progressively more severe with time. The corresponding orientation maps again confirm the localization of strain. However, two more phenomena become apparent in the orientation map sequence. The first is that significant grain growth has occurred during the AC stressing, even within the first 10 seconds. This is evident in two grains, marked A and B, which have nearly doubled in lateral size. The growth in both grains must have taken place prior to the formation of the slip lines, since the spatial extent of the slip lines exceeds the original grain sizes. The second notable feature is the partitioning of grain B into two distinct grains. The EBSD scan indicates that the new boundary shows a low misorientation angle. A Schmid factor analysis indicates that the new grain in the bottom half of the line width is starting to rotate into an orientation even more favorable for slip.

In an attempt to understand the progression of deformation, we also viewed the orientation maps of Figure 2 in terms of Schmid factors, by "applying" a load along the longitudinal direction of the line, and by considering the usual slip systems for face-centered cubic crystals. What became apparent through this analysis was the fact that grains that showed the highest resolved shear stresses were NOT necessarily the ones that yielded first. An analysis of the grain size dependence of deformed versus undeformed grains revealed the following. The average grain diameter of 25 grains that showed slip lines after 40 s of AC testing, was 3.89

μm, with a standard deviation of 0.79 μm about the mean. The average diameter of 50 grains which showed no slip line formation after 40 s of testing, was 1.83 μm, with standard deviation0.64 μm about the mean. It is apparent that larger grains are favored for deformation at the onset of testing, even if their Schmid factors are not among the highest in the grain aggregate. We are in the process of using EBSD to consider the roles of grain size and Schmid factor as weighting factors in a model for predicting slip order in AC-induced fatigue testing of small structures.

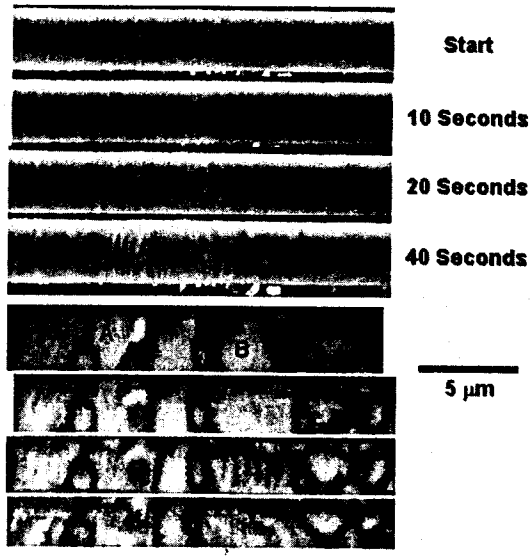

Figure 2: Damage evolution due to AC stressing of an Al-1Si line. Top four SEM images show time progression. Bottom four orientation maps correspond to the SEM images, in the same time sequence

Complicating the process is the observation of growing and shrinking grains. A preliminary analysis of 14 grains whose areas changed by at least 0.5 μm^2 after 20 s of testing revealed that growing grains had an average initial area of 6.2 μm^2 and grew to 8.7 μm^2. Those that contracted had an average initial area of 2.9 μm^2 and shrank to 2.4 μm^2. The appropriate weighting of grains whose sizes change during testing is not yet clear for a slip order model. The grain growth aspects of this work have only begun to be considered but will likely depend upon factors such as grain boundary structures, which will dictate both the grain boundary mobility as well as the effectiveness of boundaries as dislocation sources. Since grain growth is observed prior to slip line formation in some grains, it is possible that a threshold grain size is required for a given Schmid factor orientation before slip can take place. Grain re-orientation during testing should also contribute.

The value of obtaining mappings of local variations in microstructure in this quasi *in-situ* test is quite clear. We have been able to obtain detailed information about the progression of microstructural changes without compromising sample integrity. At present, plans for continuing this work include varying factors such as AC frequency and current density and consideration of the constraining effects of different encapsulating materials. TEM will also be used to clarify in detail the role of dislocations in this process.

Phase Transformation-Induced Deformation of AlGaAs/GaAs Multilayers

Initial efforts in this work targeted the use of convergent-beam electron diffraction to measure elastic strains induced by the AlGaAs to Al_2O_3 transformation. However, the strains were actually large enough to render this approach ineffective, since deficiency HOLZ lines with high symmetry zone axes in TEM changed too much for useful measurements. We then considered using EBSD to detect the strains, since we expected strains in excess of a few percent. Since there was no precedent for using this method to detect such large strains, we attempted a simple calibration by obtaining patterns from two materials with the same crystal structure but with a large difference in lattice parameters, namely GaP (a = 0.54512 nm) and GaAs (a = 0.56533 nm). Figure 3 shows the patterns obtained from these crystals, which were mounted in the SEM in approximately the same orientation. Measurement of the width of the vertical bands, (440) diffraction bands, gave a relative difference of 3.4 %, depending on the amount of image processing done to the original patterns. This compares favorably to the calculated difference in lattice parameters of 3.64 %.

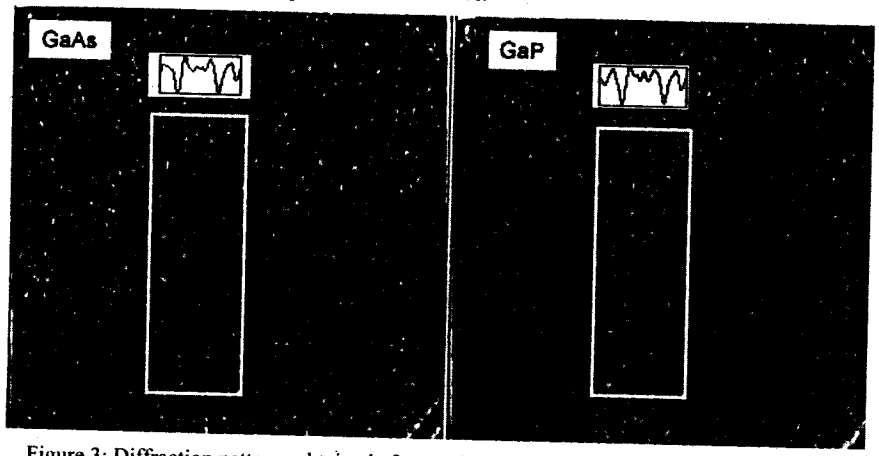

Figure 3: Diffraction patterns obtained after applying a high frequency filter to the original patterns using an FFT mask. The line scans shown in the small boxes represent the pixel intensity averaged horizontally over the height of the outlined box for the (440) Kikuchi band. The relative difference in lattice spacings of the two materials using the measured Kikuchi band widths is 3.4 %.

Based on this analysis, we proceeded with the use of EBSD to characterize the strain fields associated with oxidation in the semiconductor samples. Two approaches were used. In one, the pattern sharpness image of an automatic orientation mapping analysis was obtained on an area of approximately 1000 nm x 600 nm, processed in 20 nm steps. The results are shown in Figure 4, which qualitatively outlines a region of strain.

In the other approach, individual diffraction patterns with longer integration times were systematically taken from an oxidized region, and differences between these patterns and a reference pattern well away from the oxidized front were recorded. Diffraction patterns from a reference and from low- and high-strain areas and the differences between the latter and the reference pattern are shown in Figure 5. The distinction between the low-strain and high-strain areas is readily seen and can be used to qualitatively assess the strain field around the oxidized growth front.

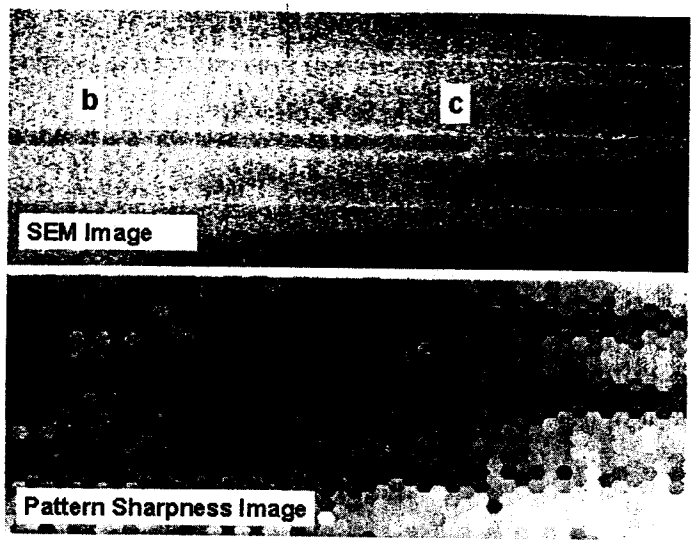

Figure 4: SEM and pattern sharpness images of the same oxidized growth front. The sharpnes image maps out the strain field around the oxidized growth front.

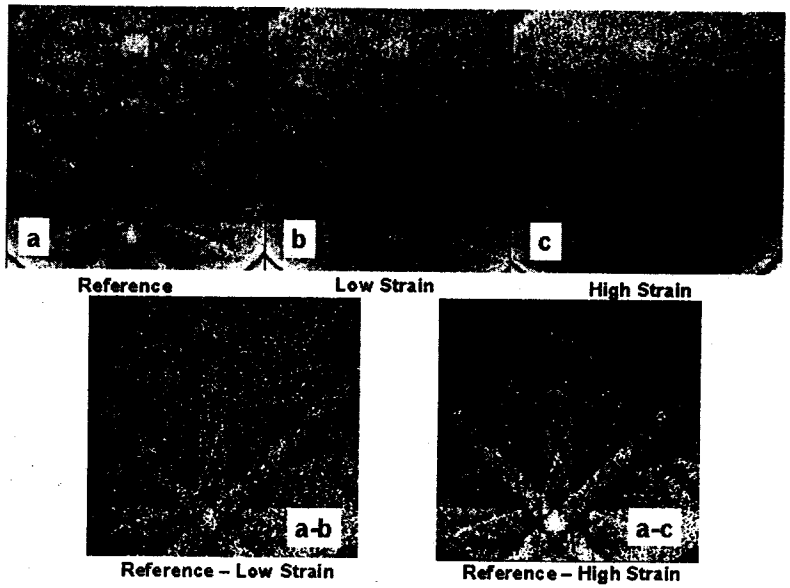

Figure 5: Original diffraction patterns from a reference, an area with low strain and an area nea the oxidized front denoted as a, b and c, respectively. (The locations of b and c are indicated in the SEM image in Figure 4. Location a is well away from the image.) The difference patterns. a-b and a-c, show clear distinctions between the levels of strain.

Summary

We have shown how electron backscatter diffraction (EBSD) has been used to study localized deformation in two types of constrained volume materials. The results of one study allowed us to formulate a mechanistic understanding of the deformation process that occurred during the deformation of narrow aluminum interconnects following low frequency, AC cycling at high current density. In the second study, we presented two different applications of EBSD to the study of elastic strains accompanying the selective oxidation of multilayered AlGaAs/GaAs structures.

Acknowledgements

We acknowledge support from the NIST Office of Microelectronics Programs and the NIST Advanced Technology Program. Valuable discussions about the AC studies with R. Mönig and C. Volkert of the Max-Planck-Institute for Metals Research are gratefully acknowledged.

References

1. P. N. Quested, P. J. Henderson, and M. McLean, "Observations of Deformation and Fracture Heterogeneities in a Nickel-Base Superalloy using Electron Back Scattering Patterns," Acta metall., 36 (1988), 2743-2752.

2. A. Day and G. Shafirstein, "Assessment of local residual strain by electron backscatter patterns and nanoindentation," Mater. Sci. Tech., 12 (1996), 873-879.

3. K. Z. Troost, "Assessment of implantation damage by backscatter Kikuchi diffraction in the scanning electron microscope," Appl. Phys. Lett., 63 (1993), 958-960.

4. A. J. Wilkinson, "Advances in SEM-based diffraction studies of defects and strains in semiconductors," J. Electron Microscopy, 49 (2000), 299-310.

5. K. Z. Troost, P. van der Sluis, and D. J. Gravesteijn, "Microscale elastic-strain determination by backscatter Kikuchi diffraction in the scanning electron microscope," Appl. Phys. Lett., 62 (1993), 1110-1112.

6. A. J. Wilkinson, "Measurement of elastic strains and small lattice rotations using electron back scatter diffraction," Ultramicroscopy, 62 (1996), 237-247.

7. J. R. Michael and J. A. Eades, "Use of reciprocal lattice layer spacing in electron backscatter diffraction pattern analysis," Ultramicroscopy, 81 (2000), 67-81.

8. J. A. Kozubowski, R. R. Keller, and W. W. Gerberich, "Effects of tetragonal distortion in thin epitaxic films on electron channelling patterns in scanning electron microscopy," J. Appl. Cryst., 24 (1991), 102-107.

9. R. R. Keller, R. Mönig, C. A. Volkert, E. Arzt, R. Schwaiger, and O. Kraft, "Interconnect Failure due to Cyclic Loading," Stress-Induced Phenomena in Metallization: Sixth International Workshop, ed. S. P. Baker, M. A. Korhonen, E. Arzt, and P. S. Ho, (Melville, NY:American Institute of Physics, 2002), 119-132.

10. R. D. Twesten, D. M. Follstaedt, K. D. Choquette, and R. P. Schneider, Jr., "Microstructure of laterally oxidized AlxGa1-xAs layers in vertical-cavity lasers," Appl. Phys. Lett., 69 (1996), 19-21.